

Observation of the critical state to multiple-type Dirac semimetal phases in KMgBi

Cite as: J. Appl. Phys. **129**, 235109 (2021); <https://doi.org/10.1063/5.0045466>

Submitted: 26 January 2021 • Accepted: 29 May 2021 • Published Online: 18 June 2021

 D. F. Liu, L. Y. Wei, C. C. Le, et al.

COLLECTIONS

Paper published as part of the special topic on [Topological Materials and Devices](#)



View Online



Export Citation



CrossMark

ARTICLES YOU MAY BE INTERESTED IN

[Transition from intrinsic to extrinsic anomalous Hall effect in the ferromagnetic Weyl semimetal \$\text{PrAlGe}_{1-x}\text{Si}_x\$](#)

APL Materials **8**, 011111 (2020); <https://doi.org/10.1063/1.5132958>

[The quantum spin Hall effect and topological insulators](#)

Physics Today **63**, 33 (2010); <https://doi.org/10.1063/1.3293411>

[Signatures of temperature driven antiferromagnetic transition in the electronic structure of topological insulator \$\text{MnBi}_2\text{Te}_4\$](#)

APL Materials **8**, 021105 (2020); <https://doi.org/10.1063/1.5142846>

Journal of Applied Physics **Special Topics** Open for Submissions

[Learn More](#)








Observation of the critical state to multiple-type Dirac semimetal phases in KMgBi

Cite as: J. Appl. Phys. 129, 235109 (2021); doi: 10.1063/5.0045466

Submitted: 26 January 2021 · Accepted: 29 May 2021 ·

Published Online: 18 June 2021



D. F. Liu,¹  L. Y. Wei,² C. C. Le,³ H. Y. Wang,² X. Zhang,²  N. Kumar,³ C. Shekhar,³  N. B. M. Schröter,⁴ Y. W. Li,² D. Pei,⁴ L. X. Xu,² P. Dudin,⁵ T. K. Kim,⁵  C. Cacho,⁵ J. Fujii,⁶ I. Vobornik,⁶  M. X. Wang,^{2,7} L. X. Yang,^{8,9} Z. K. Liu,^{2,7} Y. F. Guo,²  J. P. Hu,¹⁰ C. Felser,³ S. S. P. Parkin,¹ and Y. L. Chen^{2,4,7,8,a)} 

AFFILIATIONS

¹Max Planck Institute of Microstructure Physics, Halle 06120, Germany

²School of Physical Science and Technology, ShanghaiTech University, Shanghai 201210, China

³Max Planck Institute for Chemical Physics of Solids, Dresden D-01187, Germany

⁴Clarendon Laboratory, Department of Physics, University of Oxford, Oxford OX1 3PU, United Kingdom

⁵Diamond Light Source, Didcot OX110DE, United Kingdom

⁶CNR-IOM, TASC Laboratory in Area Science Park, 34139 Trieste, Italy

⁷ShanghaiTech Laboratory for Topological Physics, Shanghai 200031, China

⁸State Key Laboratory of Low Dimensional Quantum Physics, Department of Physics, Tsinghua University, Beijing 100084, China

⁹Frontier Science Center for Quantum Information, Beijing 100084, China

¹⁰Institute of Physics, Chinese Academy of Sciences, Beijing 100190, China

Note: This paper is part of the Special Topic on Topological Materials and Devices.

a) Author to whom correspondence should be addressed: yulin.chen@physics.ox.ac.uk

ABSTRACT

Dirac semimetals are classified into different phases based on the types of Dirac fermions. Tuning the transition among different types of Dirac fermions in one system remains a challenge. Recently, KMgBi was predicted to be located at a critical state in which various types of Dirac fermions can be induced owing to the existence of a flatband. Here, we carried out systematic studies on the electronic structure of KMgBi single crystals by combining angle-resolve photoemission spectroscopy and scanning tunneling microscopy/spectroscopy. The flatband was clearly observed near the Fermi level. We also revealed a small bandgap of ~ 20 meV between the flatband and the conduction band. These results demonstrate the critical states of KMgBi that transition among various types of Dirac fermions can be tuned in one system.

© 2021 Author(s). All article content, except where otherwise noted, is licensed under a Creative Commons Attribution (CC BY) license (<http://creativecommons.org/licenses/by/4.0/>). <https://doi.org/10.1063/5.0045466>

I. INTRODUCTION

Topological materials have been intensively studied recently, as they exhibit many unusual physical properties such as the existence of topologically protected dissipationless current and new types of fermions, such as Dirac, Weyl, and Majorana fermions, which have great potential for applications in electronic devices and quantum computing technology.^{1–4} In the past several years, the success in the discovery of various topological materials by a combination of theory and experiments, ranging from topological insulators (TIs)^{5–7} to Dirac semimetals (DSMs)^{8–14} and Weyl

semimetals (WSMs),^{15–29} has greatly enriched the topological quantum states (TQSS) of matter.

Among these TQSS, DSMs have attracted intensive attention as they host a linear Dirac cone in their electronic structures that can lead to many exotic properties.^{8,30–33} According to the Fermi surface (FS) topologies, DSMs can be classified into three types: (i) type-I DSMs host point-like FS topology;^{10,11} (ii) type-II DSMs host electron and hole Fermi pockets where the Dirac cone are strongly tilted;^{12–14} and (iii) type-III DSMs appear at the phase transition point between type-I and type-II DSMs where the Dirac

point (DP) is formed by the crossing of a strict flatband and a linear dispersion with a line-like FS topology.^{34,35} However, these three types of DSMs exist in different systems, i.e., type-I DSMs in Na₃Bi¹⁰ and Cd₃As₂¹¹ and type-II DSMs in PtSe₂ and PtTe₂,^{12–14} while type-III DSMs were predicted in Zn₂In₂S₅³⁴ and Ta₂Se₈I,³⁵ which makes it difficult to study the topological phase transition among different types of Dirac fermions.

Recently, KMgBi was theoretically predicted to be located at a critical state that all the three types of Dirac fermions can be induced owing to the existence of a flatband.³⁶ The velocity sign of the flatband can be easily tuned by applying strain or substituting K atom by Rb or Cs, leading to the realization of various types of Dirac fermions.³⁶ KMgBi was also predicted to host one-dimensional topological hinge Fermi arcs connecting the bulk three-dimensional (3D) DPs.³⁷ Here, we carried out systematic studies on the electronic structures of KMgBi single crystal by combining angle-resolved photoemission spectroscopy (ARPES) and scanning tunneling microscopy/spectroscopy (STM/STS). We revealed the complete electronic structure of KMgBi and directly observed the flatband near the Fermi level. Moreover, a small bandgap of ~20 meV between the flatband and the conduction band was also observed. These results demonstrate the critical state of KMgBi that the transitions among various types of Dirac fermions can be tuned in one system.

II. METHODS

KMgBi single crystals were grown by using the self-flux method. The K chunk (99.5%), Mg chunk (99.9%), and Bi grains (99.9%) were mixed in the stoichiometric ratio and put into an aluminum crucible and then sealed into a quartz tube with a partial pressure of argon. The assembly was slowly heated to 673 K, maintained at this temperature for 10 h, and then further heated up to 1123 K for 2 days, followed by slowly cooling down to 773 K at a temperature decreasing rate of 2–3 K/h. KMgBi single crystals with a typical size 3 × 4 × 0.3 mm³ were obtained. It should be noted that all manipulations, except the sealing and reaction, were carried out in an argon-filled glovebox. The phase and quality of KMgBi were examined on a Bruker D8 Venture single crystal x-ray diffractometer (SXRD) with Mo K_{α1} (λ = 0.710 73 Å) at 298 K. ARPES experiments were performed at beamline I05 of the Diamond Light Source (DLS) with a Scienta R4000 analyzer and beamline advanced photoelectric effect (APE) of the Elettra synchrotron with a Scienta DA30 analyzer. The sample temperature was kept as 8 and 15 K in APE and DLS, respectively. The pressure was better than 2 × 10^{−10} Torr. The angle resolution was <0.2°, and the overall energy resolution was <15 meV. The STM/STS measurement was carried out in an ultrahigh vacuum chamber with the pressure better than 2 × 10^{−10} Torr. The KMgBi sample was cleaved *in situ* in the preparation chamber at room temperature and then transferred to the STM sample stage kept at 5.2 K. A PtIr tip was used for imaging and tunneling, which has been calibrated on the sliver islands grown on p-type Si(111) 7 × 7 by means of molecule beam epitaxy (MBE). All the dI/dV curves were obtained by a lock-in technique with a 5 mV modulation at 971.2 Hz. The samples were cleaved along the (001) plane for both ARPES and STM experiments. The band calculations were performed based on the projector augmented wave method encoded in the Vienna *ab initio*

simulation package (VASP) code.^{38–40} The Perdew–Burke–Ernzerhof (PBE) exchange–correlation functional and the projector augmented wave (PAW) approach are used for the exchange–correlation potential. The cutoff energy is set to be 500 eV for expanding the wave functions into a plane wave basis. In the calculation, the Brillouin zone (BZ) is sampled in the momentum space within a Monkhorst–Pack scheme.⁴¹ On the basis of the equilibrium structure, the momentum mesh used is 10 × 10 × 6. The calculations with a hybrid functional (using HSE03)⁴² were also performed to study the ground state of KMgBi. The amount of exact Hartree–Fock exchange is set to 0.17.

III. EXPERIMENTAL RESULTS

The crystal structure of KMgBi is shown in Fig. 1(a). It crystallizes in a tetragonal structure with the space group of *P4/nmm* and is comprised of ...K–Bi–Mg₂–Bi–K... layers [Fig. 1(a)]. In each layer, the Mg atoms form a 2D square lattice with K and Bi atoms located alternatively above and below the Mg square [Fig. 1(a)]. The distance of K and Bi atoms with respect to the Mg plane are 2.927 Å and 1.724 Å, respectively [Fig. 1(a)]. The adjacent K–Bi–Mg₂–Bi–K layers are weakly coupled by the van der Waals forces, resulting in the crystal that naturally cleaves between K–K bonds that are ideal for the ARPES and STM/STS measurements.

The band structure of KMgBi is dominated by Bi-6*p* orbitals near the Fermi level, and the dispersions were calculated using two different methods as shown in Figs. 1(c) and 1(d), respectively. Both calculations reveal a flatband (labeled as α) near the Fermi level along the ΓZ direction. The flatband is dominated by the Bi-6*p*_{*x,y*} orbital and originates from the weak interaction between the two adjacent K–Bi–Mg₂–Bi–K layers along the *z* direction. generalized gradient approximation (GGA) calculations show that the flatband is linearly intersected by the conduction band (labeled as β) and the type-I Dirac fermion is formed [see the inset in Fig. 1(c)], while HSE calculations reveal a small bandgap of 16.3 meV between the flatband and the conduction band without band inversion [see the inset in Fig. 1(d)]. By applying strain or substituting a K atom by an Rb/Cs atom, such small bandgap can easily vanish, leading to the formation of the Dirac fermion.³⁶ In the meantime, the velocity sign of the flatband can also be tuned, driving the system into type-II DSM.³⁶ At the phase transition point between type-I and type-II DSM phases, type-III DSM phase can be realized where the velocity of the flatband strictly equals zero.

To investigate the electronic structure of KMgBi, we first carried out ARPES measurements on high-quality KMgBi single crystals. Figure 1(e) shows the sharp characteristic core levels of K, Mg, and Bi [Fig. 1(e)]. The broad FS mapping [Fig. 1(f)] covering multiple Brillouin zones (BZs) illustrates the overall FS topology of KMgBi, consisting of point-like FS at the center of the BZ.

Figure 2(a) illustrates the 3D volume plot of the electronic structure showing that the point-like FS at $\bar{\Gamma}$ is formed by the top of a hole band. The large-energy scale of the band dispersion along different high-symmetry directions across the whole BZ is shown in Fig. 2(b). As the overall electronic structures derived from GGA [Fig. 1(c)] and HSE [Fig. 1(d)] calculations are consistent with each other except for the relative positions of the α and β bands, to understand the experimental band structure, we performed GGA

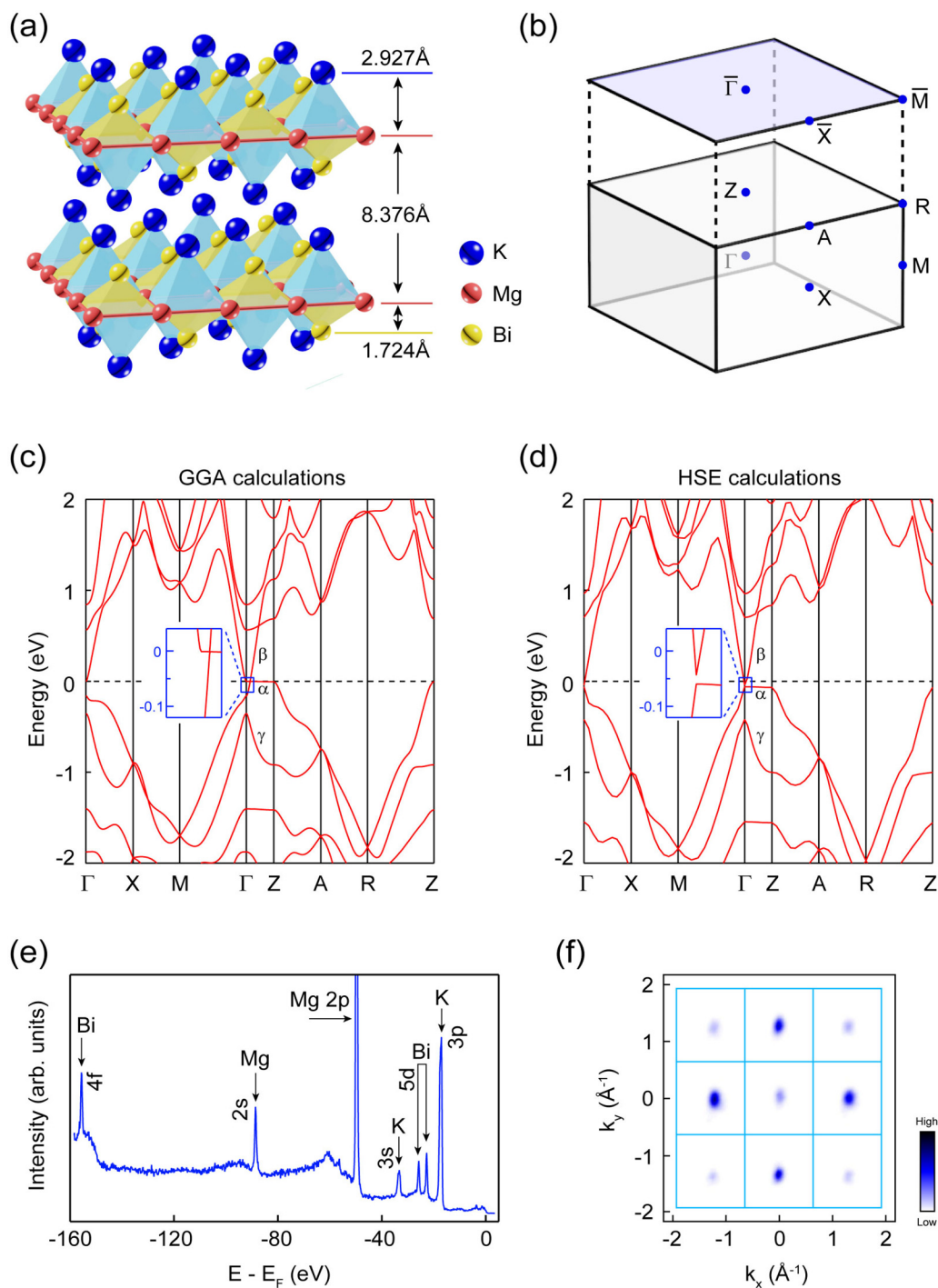


FIG. 1. The calculated electronic structure of KMgBi. (a) Schematic illustration of the crystal structure of KMgBi. (b) The 3D BZ of KMgBi and its projected surface BZ to the (001) plane. (c) and (d) Calculated bulk electronic structure of KMgBi with spin-orbit coupling (SOC) based on the GGA (c) and HSE (d) calculations. Both calculations show a flatband (labeled as α) lying near the Fermi level along the ΓZ direction. (e) The core-level photoemission spectrum of KMgBi shows sharp characteristic peaks of K, Mg, and Bi atoms. (f) Broad FS map covering multiple BZs shows the point-like FS at the center of BZ. The FS was taken by a 150 eV photon.

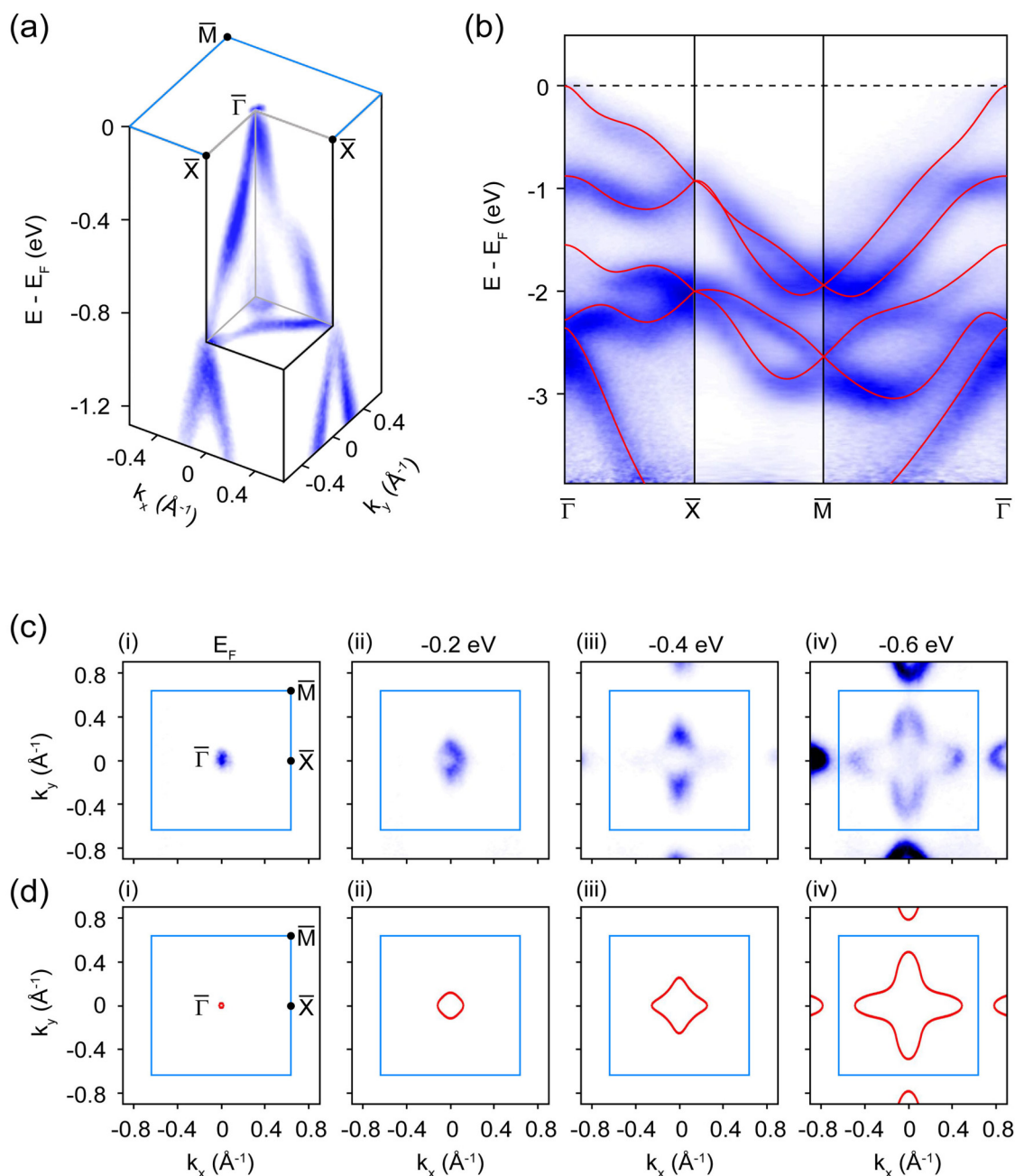


FIG. 2. The overall electronic structure of KMgBi. (a) The 3D plots of the electronic structure. (b) Comparison of the experimental and calculated (red curves) band dispersions along high-symmetry directions across the whole BZ, showing excellent agreement. (c) and (d) The comparison of the experimental (c) and calculated (d) constant energy contours at different energies, showing excellent agreement. The calculated band structure was based on the GGA calculations and the bandwidth was renormalized by a factor of 0.9. The data were taken by a 60 eV photon.

calculations and the calculated band dispersion [red curves in Fig. 2(b)] are overlaid on the experimental results showing excellent agreements. Figure 2(c) plots the experimental constant energy contours at different energies showing that the point-like FS

[Fig. 2(c)-(i)] gradually evolves into a four-petal-like feature [Figs. 2(c)-(ii)-(iv)] with decreasing the energy to -0.6 eV [Fig. 2(c)-(iv)]. Such an evolution can also be well reproduced by the calculations as shown in Fig. 2(d).

According to the GGA and HSE calculations, the flatband (α band) is located along the k_z direction as illustrated in Figs. 3(a)-(i) and (ii), respectively. To search for the flatband, we performed detailed photon energy dependent measurements (20–90 eV) along the k_z direction as shown in Fig. 3(b). The spectra intensity map at

the Fermi level in the k_y - k_z plane [Fig. 3(b)] shows a vertical line-like FS along the ΓZ direction. Figures 3(c)-(i) and (ii) are the extracted band dispersions along the ΓZ direction measured by linear horizontal (LH) and linear vertical (LV) polarizations of the photons, respectively. Under LH polarization [Fig. 3(c)-(i)], the γ

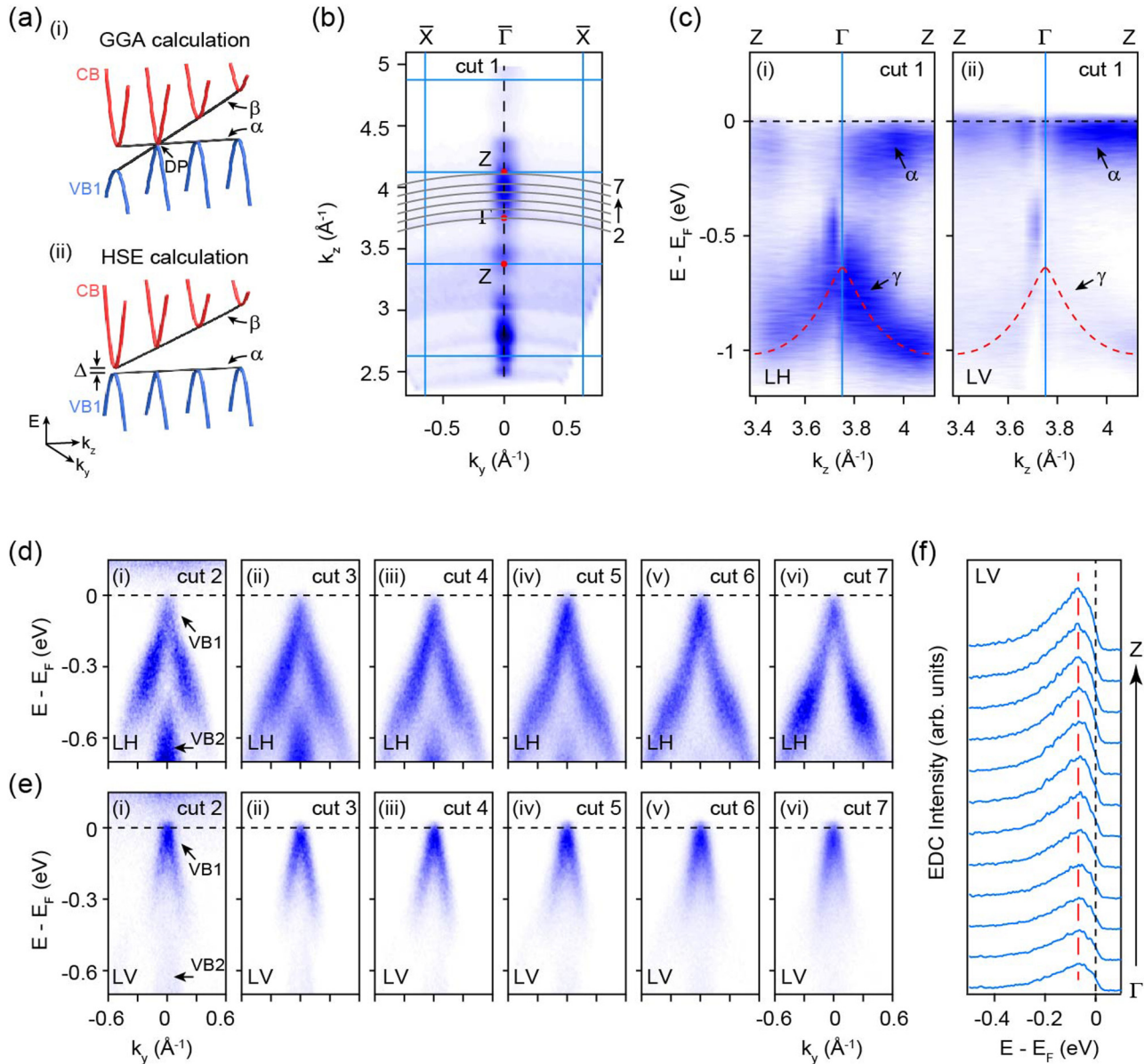


FIG. 3. Observation of the flatband. (a) Schematic illustration for the formation of the flatband (labeled as α) based on the GGA (i) and HSE (ii) calculations. (b) The spectra intensity map at the Fermi level in the k_y - k_z plane was taken by 20–90 eV photons under LH polarization. (c) The extracted band dispersion along the ΓZ direction under LH (i) and LV (ii) polarizations. (d) The band dispersion at different k_z from Γ to Z points measured under LH polarization. The corresponding k_z is shown by the gray line in (b). (e) Same as (d) but measured under LV polarization. (f) The extracted energy distribution curves (EDCs) at different k_z (3.77–4.1 \AA^{-1}) along the ΓZ direction. The red dashed line is the guideline for the peak position.

band located within the energy range of -0.5 to -1 eV was clearly resolved [see the red dashed curves in Fig. 3(c)-(i)], which is consistent with the calculations [Figs. 1(c) and 1(d)], while it was suppressed under LV polarization [Fig. 3(c)-(ii)] due to the matrix element effect. Near the Fermi level, a nondispersive flatband was observed under both polarizations [Fig. 3(c)] as illustrated in Fig. 3(a).

The flatband can also be visualized from the dispersions at different k_z from Γ to Z points as shown in Figs. 3(d) and 3(e). The VB1 band's top lies near the Fermi level and the positions under both polarizations are unchanged upon varying k_z [Figs. 3(d) and 3(e)], as expected for the flatband. At energy of -0.6 eV, the VB2 band was only observed under LH polarization [Fig. 3(d)-(i)] due to the matrix element effect. Its top position gradually moves down [Figs. 3(d)-(i)-(vi)] forming the γ band [Fig. 3(c)-(i)] upon varying k_z from Γ to Z points. Figure 3(f) shows the EDCs extracted at different k_z along the ΓZ direction. The peak position does not change upon varying k_z , again suggesting the dispersionless nature of the flatband.

GGA calculations show KMgBi is a DSM [Fig. 1(c)], while HSE calculations show it is a semiconductor [Fig. 1(d)]. In a DSM, the density of state (DOS) is finite and becomes minimal at

the DP, while it has a zero DOS at the Fermi level due to the formation of a full bandgap in a semiconductor. To determine the ground state of KMgBi, we performed high-resolution STM/STS measurements as shown in Fig. 4. The large-scale topography map [Fig. 4(a)] exhibits inhomogeneous local DOS on the surface of the cleaved KMgBi sample. The STS spectra on the high DOS region (marked by the purple line in Fig. 4(a)) were systematically studied as shown in Fig. 4(b). A gap structure is clearly observed at the Fermi level, characterized by the low intensity of the dI/dV spectra. We also studied the STS spectra on the low DOS region [Fig. 4(c)], and a similar gap structure was also observed [Fig. 4(d)]. The large variation of the dI/dV spectra [Figs. 4(b) and 4(d)] may be caused by the impurities and defects, for example, the intrinsic Bi impurities and K vacancies, as well as the possible oxidization, since KMgBi is very sensitive. To quantitatively determine the gap size, we selected several points on the sample surface (red and green circles in Figs. 4(a) and 4(c)), and the corresponding STS spectra are shown in Fig. 4(e). Although the dI/dV spectra show large variation, all the dI/dV spectra show a bulk bandgap of ~ 20 meV, demonstrating the semiconducting state of KMgBi. Our results are consistent with the HSE calculations and the transport measurement.⁴³

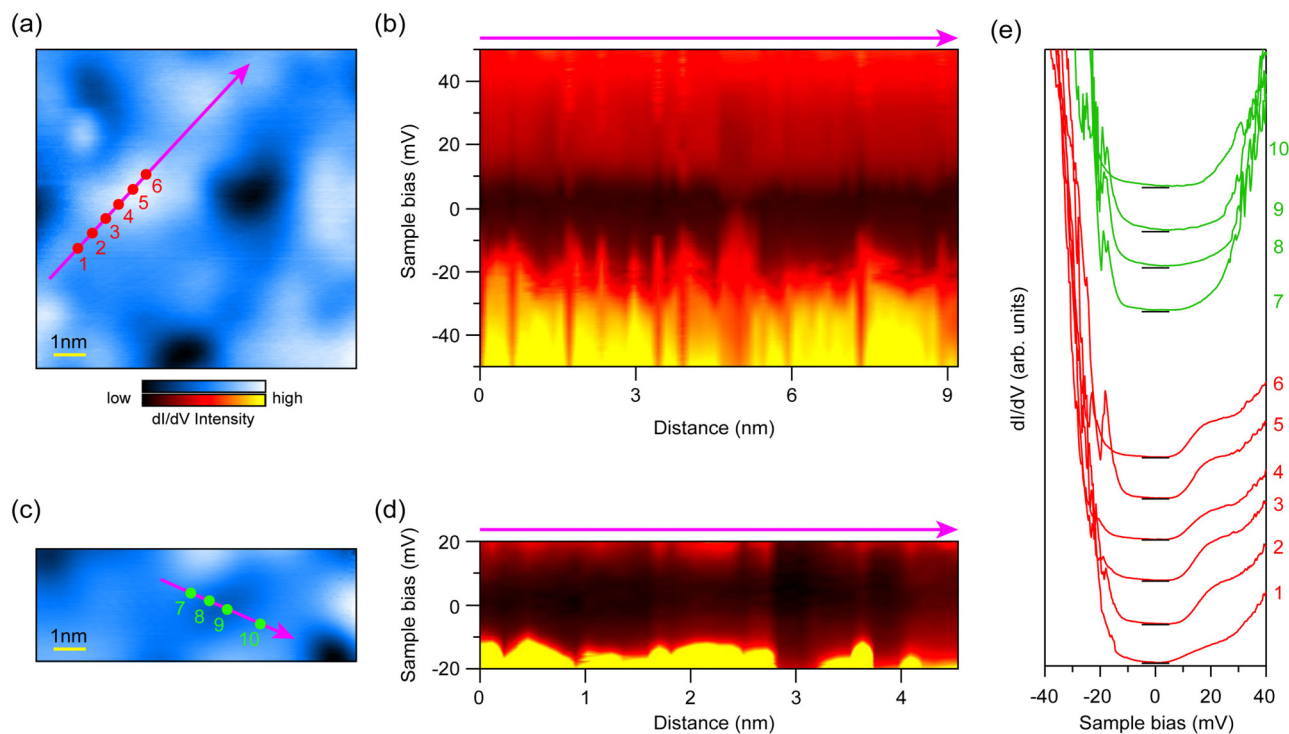


FIG. 4. Observation of a small semiconducting gap in KMgBi. (a) Large-scale scan on the surface of the cleaved KMgBi single crystal showing inhomogeneous local DOS. (b) STS spectra on the high DOS region illustrated by the purple line in (a). (c) The STM image of the low DOS region illustrated by the purple line in (c). (d) STS spectra on the low DOS region illustrated by the purple line in (c). (e) STS spectra taken on several surface locations. The red curves were taken on the high DOS region and the corresponding positions are illustrated by the red circles in (a). The green curves were taken on the low DOS region and the corresponding positions are illustrated by the green circles in (c). The STS spectra are offset for clarity. The black bars are the zero dI/dV intensity for each STS spectrum. They all show a full gap of ~ 20 meV at the Fermi level, demonstrating the semiconducting state of KMgBi.

IV. DISCUSSION

The inaccuracy of the GGA calculations in describing the ground state of KMgBi is caused by the inadequacy in describing the energy gap size between the valence and conduction bands due to the existence of a derivative discontinuity of the energy with respect to the number of electrons.⁴⁴ The HSE calculations with inclusion of a certain amount of Hartree–Fock exchange can well capture the bandgap of KMgBi. According to the HSE calculations, such a small bandgap can be easily manipulated to drive KMgBi into DSM phases with different types of Dirac fermions,³⁶ i.e., KMgBi can be turned into type-I DSM by applying out-of-plane tensile strain, while type-II DSM can be induced by applying in-plane compressive strain or by doping Rb or Cs; type-III DSM can also be realized at the topological phase transition point between type-I and type-II DSM phases. We note that a resistivity plateau was observed in the transport measurement that was attributed to the existence of a nontrivial topological surface state.⁴³ However, all the observed electronic structures in our experiments are bulk states without any indications of the surface state indicating that the resistivity plateau is more likely caused by the impurity.

V. CONCLUSIONS

In summary, we have performed systematic studies on the electronic structure of KMgBi single crystals by combining ARPES and STM/STS. The flatband and a small bandgap of ~ 20 meV between the flatband and the conduction band were clearly observed. These results demonstrate the critical state of KMgBi that the transitions among various types of Dirac fermions can be tuned in one system.

AUTHORS' CONTRIBUTIONS

D.F.L. and L.Y.W. contributed equally to this work.

ACKNOWLEDGMENTS

This work has been performed in diamond light source (SI18005-1) and in the framework of the nanoscience foundry and fine analysis (NFFA-MIUR Italy, Progetti Internazionali) facility. Z. K. Liu acknowledges the National Key R&D program of China (Grant No. 2017YFA0305400) and the Shanghai Technology Innovation Action Plan 2020-Integrated Circuit Technology Support Program (Project No. 20DZ1100605). C. Felser acknowledges the support from the European Research Council (ERC) Advanced Grant No.742068 (“TOPMAT”), Deutsche Forschungsgemeinschaft (DFG) under SFB1143 (Project No. 247310070), and Würzburg-Dresden Cluster of Excellence on Complexity and Topology in Quantum Matter-ct.qmat (EXC 2147, Project No. 39085490). D. Pei acknowledges the sponsor from the China Scholarship Council (CSC). Y.W.L. acknowledges the

support from International Postdoctoral Exchange Fellowship Program (Talent-Introduction Program, Grant No. YJ20200126).

DATA AVAILABILITY

The data that support the findings of this study are available within the article.

REFERENCES

- ¹M. Z. Hasan and C. L. Kane, *Rev. Mod. Phys.* **82**, 3045 (2010).
- ²N. P. Armitage, E. J. Mele, and A. Vishwanath, *Rev. Mod. Phys.* **90**, 015001 (2018).
- ³X.-L. Qi and S.-C. Zhang, *Rev. Mod. Phys.* **83**, 1057 (2011).
- ⁴S. R. Elliott and M. Franz, *Rev. Mod. Phys.* **87**, 137 (2015).
- ⁵H. Zhang *et al.*, *Nat. Phys.* **5**, 438–442 (2009).
- ⁶D. Hsieh *et al.*, *Nature* **452**, 970–974 (2008).
- ⁷Y. L. Chen *et al.*, *Science* **325**, 178–181 (2009).
- ⁸Z. Wang *et al.*, *Phys. Rev. B* **85**, 195320 (2012).
- ⁹Z. Wang *et al.*, *Phys. Rev. B* **88**, 125427 (2013).
- ¹⁰Z. K. Liu *et al.*, *Science* **343**, 864–867 (2014).
- ¹¹Z. K. Liu *et al.*, *Nat. Mater.* **13**, 677–681 (2014).
- ¹²M. Yan *et al.*, *Nat. Commun.* **8**, 257 (2017).
- ¹³K. Zhang *et al.*, *Phys. Rev. B* **96**, 125102 (2017).
- ¹⁴Y. Li *et al.*, *Phys. Rev. Mater.* **1**, 074202 (2017).
- ¹⁵H. Weng *et al.*, *Phys. Rev. X* **5**, 011029 (2015).
- ¹⁶S.-Y. Xu *et al.*, *Science* **349**, 613–617 (2015).
- ¹⁷B. Q. Lv *et al.*, *Phys. Rev. X* **5**, 031013 (2015). doi:
- ¹⁸L. X. Yang *et al.*, *Nat. Phys.* **11**, 728–732 (2015).
- ¹⁹A. A. Soluyanov *et al.*, *Nature* **527**, 495–498 (2015).
- ²⁰Y. Sun *et al.*, *Phys. Rev. B* **92**, 161107(R) (2015).
- ²¹Z. Wang *et al.*, *Phys. Rev. Lett.* **117**, 056805 (2016).
- ²²K. Deng *et al.*, *Nat. Phys.* **12**, 1105–1110 (2016).
- ²³A. Tamai *et al.*, *Phys. Rev. X* **6**, 031021 (2016). doi:
- ²⁴J. Jiang *et al.*, *Nat. Commun.* **8**, 13973 (2017).
- ²⁵E. Liu *et al.*, *Nat. Phys.* **14**, 1125–1131 (2018).
- ²⁶Q. Xu *et al.*, *Phys. Rev. B* **97**, 235416 (2018).
- ²⁷D. F. Liu *et al.*, *Science* **365**, 1282–1285 (2019).
- ²⁸N. Morali *et al.*, *Science* **365**, 1286–1291 (2019).
- ²⁹I. Belopolski *et al.*, *Science* **365**, 1278–1281 (2019).
- ³⁰M. Koshino *et al.*, *Phys. Rev. B* **81**, 195431 (2010).
- ³¹W. Zhang *et al.*, *Phys. Rev. Lett.* **106**, 156808 (2011).
- ³²C.-X. Liu *et al.*, *Phys. Rev. B* **81**, 041307(R) (2010).
- ³³C. Zhang *et al.*, *Nature* **565**, 331–336 (2019).
- ³⁴H. Huang *et al.*, *Phys. Rev. B* **98**, 121110(R) (2018).
- ³⁵X.-P. Li *et al.*, *arXiv:1909.12178*.
- ³⁶C. Le *et al.*, *Phys. Rev. B* **96**, 115121 (2017).
- ³⁷B. J. Wieder *et al.*, *Nat. Commun.* **11**, 627 (2020).
- ³⁸G. Kresse and J. Hafner, *Phys. Rev. B* **47**, 558 (1993).
- ³⁹G. Kresse and J. Furthmüller, *Comput. Mater. Sci.* **6**, 15 (1996).
- ⁴⁰G. Kresse and J. Furthmüller, *Phys. Rev. B* **54**, 11169 (1996).
- ⁴¹H. J. Monkhorst and J. Pack, *Phys. Rev. B* **13**, 5188 (1976).
- ⁴²J. Heyd, G. E. Scuseria, and M. Ernzerhof, *J. Chem. Phys.* **118**, 8207 (2003).
- ⁴³X. Zhang *et al.*, *Phys. Rev. B* **95**, 035209 (2017).
- ⁴⁴H. Xiao *et al.*, *J. Phys. Chem. Lett.* **2**, 212–217 (2011).